Expected Performances of the NOMAD/ExoMars instrument

Planetary and Space Science 124 (2016) 94–104

Contents lists available at ScienceDirect

Planetary and Space Science

journal homepage: www.elsevier.com/locate/pss

Expected performances of the NOMAD/ExoMars instrument

S. Robert [a,*], A.C. Vandaele [a], I. Thomas [a], Y. Willame [a], F. Daerden [a], S. Delanoye [a], C. Depiesse [a], R. Drummond [a,b], E. Neefs [a], L. Neary [a], B. Ristic [a], J. Mason [c], J.-J. Lopez-Moreno [d], J. Rodriguez-Gomez [d], M.R. Patel [c,e], G. Bellucci [f], The NOMAD Team

[a] Belgian Institute for Space Aeronomy, Brussels, Belgium
[b] IndoSpace Ltd., Abingdon, Oxon, UK
[c] Open University, Milton Keynes, UK
[d] Instituto de Astrofisica de Andalucia CSIC, Granada, Spain
[e] Rutherford Appleton Laboratory, Harwell, Oxfordshire, UK
[f] Istituto di Astrofisica e Planetologia Spaziali, Roma, Italy

ARTICLE INFO

Article history:
Received 1 December 2015
Received in revised form
18 February 2016
Accepted 3 March 2016
Available online 10 March 2016

Keywords:
ExoMars ESA mission
NOMAD instrument
Mars, atmosphere
Abundances
Radiative transfer

ABSTRACT

NOMAD (Nadir and Occultation for MArs Discovery) is one of the four instruments on board the ExoMars Trace Gas Orbiter, scheduled for launch in March 2016. It consists of a suite of three high-resolution spectrometers – SO (Solar Occultation), LNO (Limb, Nadir and Occultation) and UVIS (Ultraviolet and Visible Spectrometer). Based upon the characteristics of the channels and the values of Signal-to-Noise Ratio obtained from radiometric models discussed in (Vandaele et al., 2015a, 2015b; Thomas et al., 2016), the expected performances of the instrument in terms of sensitivity to detection have been investigated. The analysis led to the determination of detection limits for 18 molecules, namely CO, H_2O, HDO, C_2H_2, C_2H_4, C_2H_6, H_2CO, CH_4, SO_2, H_2S, HCl, HCN, HO_2, NH_3, N_2O, NO_2, OCS, O_3. NOMAD should have the ability to measure methane concentrations < 25 parts per trillion (ppt) in solar occultation mode, and 11 parts per billion in nadir mode. Occultation detections as low as 10 ppt could be made if spectra are averaged (Drummond et al., 2011). Results have been obtained for all three channels in nadir and in solar occultation.

1. Introduction

The ExoMars Trace Gas Orbiter is a joint ESA-Roscosmos mission consisting of an orbiter and an entry, descent and landing demonstrator. The mission is scheduled for launch in March 2016 and shall begin its nominal science mission around Mars in late 2017. The science mission will continue until at least 2019, covering an entire Martian year. NOMAD is one of four instruments on board the orbiter. It consists of a suite of three high-resolution spectrometers – SO (Solar Occultation), LNO (Limb, Nadir and Occultation) and UVIS (Ultraviolet and Visible Spectrometer).

The three spectrometers cover the ultraviolet, visible and infrared ranges, operating in solar occultation, limb and nadir-viewing modes, and will generate a huge dataset of Martian atmospheric observations during the mission across a wide spectral range (Neefs et al., 2015).

An order-of-magnitude increase in spectral resolution over previous instruments will allow NOMAD to achieve its three main science objectives (Vandaele et al., 2015a). These concern the chemical composition, the climatology and seasonal cycles and the sources and sinks of trace gases. NOMAD will allow us to extend existing datasets by characterizing the Martian atmosphere over the course of an entire Martian year.

It is crucial to develop tools for the data treatment and for the spectral analysis of the wealth of data that will be produced by the instrument. One important issue is to determine the levels of detection for the different possible targets, and to derive optimal observation parameters (specific spectral interval, integration times, accumulations, etc.).

The radiometric model of an instrument is critical for an accurate understanding of its characteristics and to correctly determine its expected performances. The analysis based on the knowledge of the incoming radiation and that of the theoretical transmittance/reflectance of each of the elements of the instrument has been performed. Signal to noise ratios (SNR) were then calculated and were used further to investigate the sensitivity of the instrument (Vandaele et al., 2015b; Thomas et al., 2016). Detection limits were deduced from simulated spectra, using the latest characteristics of each channel.

The three spectrometers of the NOMAD instrument will be briefly described in the next section. The methodology to investigate their

* Corresponding author.
E-mail address: severine.robert@aeronomie.be (S. Robert).

http://dx.doi.org/10.1016/j.pss.2016.03.003

performances in terms of sensitivity is presented. This study led to the determination of detection limits for 18 target molecules.

2. The NOMAD instrument

NOMAD, the "Nadir and Occultation for MArs Discovery" spectrometer suite (Neefs et al., 2015) was selected as part of the payload of the ExoMars Trace Gas Orbiter mission 2016. The instrument will conduct a spectroscopic survey of Mars' atmosphere in UV, visible and IR wavelengths covering the 0.2–0.65 and 2.3–4.3 μm spectral ranges. NOMAD is composed of 3 channels: a solar occultation channel (SO) operating in the infrared wavelength domain, a second infrared channel observing nadir, but also able to perform solar occultation and limb observations (LNO), and an ultraviolet/visible channel (UVIS) that can work in all observation modes. The spectral resolution of SO and LNO surpasses previous space-based surveys in the infrared by more than one order of magnitude. NOMAD offers an integrated instrument combination of a flight-proven concept (SO is a copy of SOIR on Venus Express) (Mahieux et al., 2009; Vandaele et al., 2008), and innovations based on existing and proven instrumentation (LNO is based on SOIR on board Venus Express (VEx) and UVIS has heritage from the ExoMars Humboldt lander [Patel et al., 2007]), that will provide mapping and vertical profile information at high spatio-temporal resolution.

Both SO and LNO consist of an echelle grating in combination with an acousto-optic tunable filter (AOTF): the dispersive element provides the spectral discrimination, while the filter selects the diffraction order (Neefs et al., 2015). An infrared detector array is actively cooled in order to maximize the signal-to-noise ratio (SNR) as much as possible.

UVIS is a copy of the miniature grating spectrometer originally designed for the ExoMars Humboldt lander with two added telescopes for measurements from orbit. UVIS can operate in solar occultation, limb, and nadir observational modes (Patel et al., 2007).

The design of the three channels has been fully described in Vandaele et al. (2015b) and in Thomas et al. (2016) for the UVIS channel and the IR channels respectively. The main characteristics are given in Table 1.

Thanks to its high spectral resolution NOMAD will be able to map previously unresolvable gas species, such as important trace gases and isotopologues. CO_2, CO, H_2O, C_2H_2, C_2H_4, C_2H_6, H_2CO, CH_4, SO_2, H_2S, HCl, HCN, HO_2, NH_3, N_2O, NO_2, OCS, O_3. The detection of several isotopologues of methane and water will provide crucial measurements of the Martian *D*/*H* ratios. It will also be possible to map the sources and sinks of these gases, such as regions of surface volcanism/outgassing and atmospheric production, over the course of an entire Martian year, to further constrain atmospheric dynamics and climatology. NOMAD will also continue to monitor the Martian water, carbon, ozone and dust cycles, extending existing datasets made by successive space missions in the past decades. Using SO and LNO in combination with UVIS, aerosol properties such as optical depth, composition and size distribution can be derived for atmospheric particles and for distinguishing dust from ice aerosols.

3. NOMAD performances

A preliminary sensitivity study (Drummond et al., 2011) was carried out to assess the detection limits using a SOIR-type instrument for solar occultation and nadir. This showed that methane concentrations below 1 ppb can be detected from just one spectrum, for a signal to noise ratio based on the SNR values currently observed with SOIR/VEx (Mahieux et al., 2009). Using the latest optical models of the three NOMAD channels, the SNR achievable have been obtained in Vandaele et al. (2015b) for the UV channel and in Thomas et al. (2016) for the IR channels. These SNR values will be used here to determine updated detection limits. Note however that these are still models that might be modified after calibration will have been performed either in the laboratory or in flight.

Although the treatment is different for solar occultation and nadir observations, the philosophy to determine the detection limits is the same: simulate a series of spectra with known abundances of the target species, add noise corresponding to the SNR considered, apply a retrieval method to fit the abundances, compare with the input values. We will detail the procedure for both solar occultation and nadir observations, and for all 3 channels.

All simulations of the spectra have been performed using the ASIMUT-ALVL radiative code developed at IASB-BIRA (Vandaele et al., 2006). Initially developed for Earth observation missions (IASI and ACE-FTS), the code was later adapted for planetary atmospheres, in particular for Venus (Vandaele et al., 2008) and Mars (Drummond et al., 2011). ASIMUT-ALVL is a modular program for radiative transfer calculations in planetary atmospheres. This code has been developed with the objective to be as general as possible, accepting different instrument types (Fourier Transform Spectrometers, grating spectrometers, AOTF combined with an echelle grating) and different geometries (nadir, ground-based, solar occultation/limb). The different contributing sources of radiation such as the Sun (direct or reflected illumination from the surface), surface emission and thermal atmospheric emission are taken into account. The spectra can be simulated in the IR and in the UV as well. The surface is considered by default to be Lambertian, but a more complex treatment is possible as well. The

Table 1
Characteristics of the NOMAD channels. Details are available in (Neefs et al., 2015; Vandaele et al., 2015a, 2015b; Thomas et al., 2016).

Channel	SO	LNO		UVIS	
Geometry	Solar occultation	Solar occultation	NADIR	Solar occultation	NADIR
Spectral range	2.2–4.3 μm (2325–4545 cm^{-1})	2.2–3.8 μm (2631–4545 cm^{-1})		200–650 nm	
Spectral resolution	0.15–0.2 cm^{-1}	0.3 cm^{-1}		1.5 nm	
Vertical spatial resolution (SO)	180–1000 m	180–1000 m	–	$<$ 300 m (Δz at limb)	–
Ground resolution (nadir)	–	–	60×17.5 km^2 for a typical 15 s observation (0.5×17.5 km^2 IFOV)	–	5×60 km^2 for a typical 15 s observation (5×5 km^2 IFOV)
Relative SNR	2000–2800	3000	100	230–450 nm: SNR $\geq$ 1000 450–650 nm: SNR $\geq$ 500	230–450 nm: SNR $\geq$ 500 450–650 nm: SNR $\geq$ 250
Measurement cycles	6 spectral domains in 1 s	6 spectral domains in 1 s	2–4 spectral domains in 15 s	Whole spectral domain in $<$ 1 s	whole spectral domain in 15 s

determination of the radiation path through the atmosphere, i.e. the path followed by the radiation reaching the instrument, requires that the planet's curvature and refraction be taken into account. The model is based on the ray-tracing program FSCATM (Gallery et al., 1983). ASIMUT-ALVL has been coupled to SPHER/TMATRIX (Mishchenko and Travis, 1998) and LIDORT (Spurr, 2006) codes (Kochenova et al., 2011) to include the complete treatment of the scattering effects into the radiative transfer calculations. Aerosols are included in the ASIMUT code, either as extinction (ASIMUT) or full scattering species (ALVL, through the call to LIDORT). The main retrieval module is based on the Optimal Estimation Method (OEM) (Rodgers, 2000) coupled to the analytical calculation of the Jacobians. It enables to fit simultaneously or sequentially different parts of one or more spectra, to fit the surface temperature, to fit columns or vertical profiles for molecular species or for aerosols and to fully characterize the outputs (averaging kernels, errors, DOFS, etc.). It is however also possible to use the more conventional Levenberg–Marquardt method for the inversion of spectra. ASIMUT-ALVL is as the reference code for the NOMAD instrument selected to be on board the ExoMars TGO. More details about this algorithm can be found on the website of IASB-BIRA (http://planetary.aeronomie.be/en/asimut_documentation/html/index.html).

First of all a reference atmosphere has been built for Mars based on the latest observations of the atmosphere composition. The core of this reference atmosphere are vertical profiles provided by the GEM Mars GCM developed at IASB-BIRA (Daerden et al., 2015). Global annual profiles for the temperature, pressure, CO_2, H_2O, O_3 as well as dust extinction are given from the surface up to 130 km. The other constituents, listed in Table 2, have been included into the model considering constant with altitude volume mixing ratio (vmr) profiles with the abundance given in Column 2 of Table 2.

Spectra are then simulated considering the following parameters or conditions:

Table 2
Reference composition and initial volume mixing ratio (vmr) values for the sensitivity study in the case of solar occultation and nadir observations. The values used for the reference atmosphere are based on the observations or detection limits found in the literature (Formisano et al., 2004; Krasnopolsky et al., 2004; Mumma et al., 2009; Fedorova et al., 2009; Smith, 2004; Smith et al., 2009; Krasnopolsy, 1997; Lodders and Fegley, 1997; Owen et al., 1977; Hartogh et al., 2010; Villanueva et al., 2013; Maguire, 1977; Lefevre et al., 2004; Perrier et al., 2006; Krasnopolsky, 2005; Encrenaz et al., 2011; Nakagawa et al., 2009; Mahaffy et al., 2013).

Species	Reference atmosphere	Initial vmr values for the SNR study in solar occultation		Initial vmr values for the SNR study in nadir	
		SO and LNO	UVIS	LNO	UVIS
CH_4	10 ppb	0.3 ppb		100 ppb	
H_2O	Global avg profile	100 ppb H_2O		100 ppb H_2O	
HDO	Global avg profile	10 ppm H_2O		10 ppm H_2O	
CO	500 ppm	1 ppm		10 ppm	
HCl	1 ppb	1 ppb		100 ppb	
HCN	3 ppb	3 ppb		100 ppb	
H_2CO	1 ppb	0.3 ppb	50 ppb	100 ppb	2000 ppb
HO_2	10 ppb	10 ppb		1 ppm	
H_2S	10 ppb	20 ppb		100 ppb	
C_2H_2	1 ppb	0.3 ppb		100 ppb	
C_2H_4	10 ppb	3 ppb		500 ppb	
C_2H_6	10 ppb	0.3 ppb		100 ppb	
OCS	1 ppb	10 ppb		100 ppb	
N_2O	10 ppb	10 ppb		100 ppb	
NO_2	1 ppb	10 ppb		100 ppb	
SO_2	1 ppb		1 ppb	–	300 ppb
O_3	Global avg profile	10 ppb	0.1 ppb	10 ppb	100 ppb
NH3	1 ppb		1 ppb	–	5000 ppb

- SO channel : Gaussian resolution of 0.15 cm^{-1}; 2.3–4.3 μm;
- LNO channel: Gaussian resolution of 0.3 cm^{-1}; 2.3–3.8 μm;
- UVIS channel: Gaussian resolution of 1.2 nm; 200–650 nm;
- UV cross sections – the following molecules were considered, see also Fig. 1 where the selected data are shown. When available the temperature dependence of the cross section is taken into account.
  - CO_2: The data from Huestis and Berkowitz (2011) has been selected since it covers a wide spectral interval at relatively high resolution. They are in very good agreement with the data of Parkinson et al. (2003) obtained at 295 K;
  - H_2CO cross section is based on the temperature dependent relation established by Meller and Moortgat (2000) corrected however for a wavelength shift in order to be in better agreement with the high resolution data from Chance and Orphal (2011);
  - NH_3 data are from Cheng et al. (2006);
  - SO_2 absorption cross section is the combination of two data sets (Danielache et al., 2008; Hermans et al., 2009; Vandaele et al., 2009) to cover the complete UVIS spectral interval;
  - O_3 has been built around the temperature dependent data sets of Serdyuchenko et al. (2014), extending the cross sections towards the shorter wavelength by using either the Reims data set (Brion et al., 1993; Daumont et al., 1992; Malicet et al., 1995) or the JPL compilation (Sander et al., 2011) depending on the temperature.
- IR spectroscopic parameter from HITRAN 2012 (Rothman et al., 2013). However, broadening coefficients have been modified in order to take into account the presence of CO_2 as the main buffer gas, whereas data reported in HITRAN are given for Earth like air conditions. Details on modifications introduced in the spectroscopic parameters line list can be found in Vandaele et al. (2008).
- Rayleigh scattering from (Sneep and Ubachs (2005);
- Solar irradiance : from the latest results of the SOLSPEC mission (Bolsée, 2012, in preparation) for the UV range, ACE-FTS data (Hase et al., 2010) for the IR;
- Abundances : for each of the species considered in this sensitivity analysis, a starting value was chosen being much higher than the expected detection limit. This value, indicated in Table 2 for the different channels and for the two observation modes, was multiplied by a series of factors covering the [100–0.001] interval (34 different values for all solar occultation, 50 for nadir-LNO, and 16 for nadir–UVIS). These were the abundances used for the simulations of spectra.

Aerosols have not been taken into account in this study. To mitigate the impact of this decision, tangent altitude and SNR have been chosen carefully. Our choices are explained in more details hereafter.

Although aerosols can be simulated by ASIMUT-ALVL, even considering their full scattering impact, we have decided to perform all the current sensitivity analysis without aerosols. The detection values obtained in this study, though using the worst case SNR values, are yet to be considered as best values, since the presence of aerosols will have as main consequence to deteriorate the retrieval. The scattering impact of dust and aerosols on the signal recorded during solar occultations can be neglected. Moreover, for the IR channel LNO, since the signal is recorded on small intervals ($\sim$20–25 cm^{-1}), the influence of aerosols/dust would be visible as a general decrease of the background of the signal. This is what is observed with SOIR/Venus Express and is at the core idea of the aerosols optical depth determination (Wilquet et al., 2009, 2012). In the UV region, the impact of aerosols is complicated by the fact that both the signature of dust/aerosols and that of the target species are broad. In nadir viewing, the scattering effect of dust/aerosols cannot be neglected. However including the full scattering properties, whilst possible with ASIMUT-

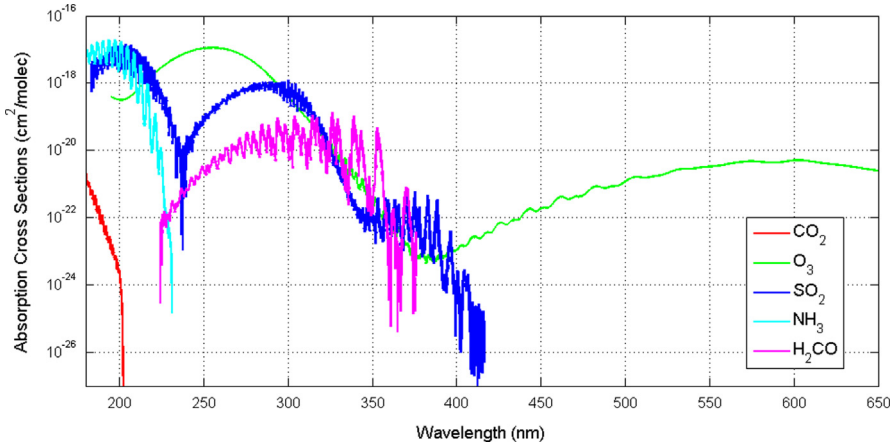

Fig. 1. Absorption cross sections of CO_2, H_2CO, NH_3, SO_2, and O_3 considered in this study.

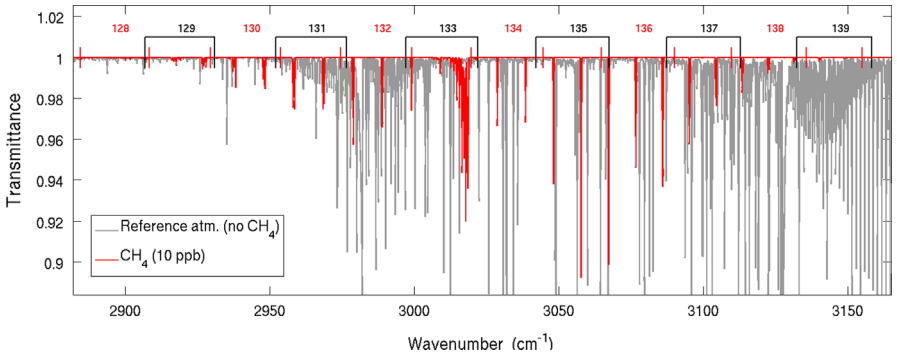

Fig. 2. Example of simulated transmittances obtained during a typical solar occultation measurement, at 20 km altitude, with the SO channel. The reference atmosphere contain the molecules in abundances presented in Table 2 while the methane spectrum is obtained with an abundance of 10 ppb. The limits of the diffraction orders covered are shown at the top of the Figure. (For interpretation of the references to color in this figure legend, the reader is referred to the web version of this article.)

ALVL, would make the process much more complex and time consuming. The analysis should then be done for different dust loadings, different solar illumination angles, etc. This will be the subject of a future investigation, whilst the objective of the present study is not a full sensitivity study of the dust on the retrieval, but only the determination of estimates of detection limits that could be derived in the best conditions. As already indicated, we are aware that this is an indication (at least for the nadir geometry) of the optimal theoretical performances of the instrument. Occultation spectra were simulated to correspond to a tangent altitude of 20 km. This is again an intentional compromised choice: the lower the tangent altitude, the longer the Line of Sight, the stronger the absorption signature. However due to the presence of dust and clouds, lower tangent altitudes will be more impacted by aerosols.

Noise was then added to all the simulated spectra. The noise level is directly related to the SNR values that were obtained during the radiometric modelling studies performed as a first step to characterize the instrument [Thomas et al. 2016]. This model operates in radiometric units. For SO (solar occultation only), the detection limits have been determined assuming a one-second cycle with 6 different spectral windows of 160 ms. From Thomas et al. (2016), we see that the study of idealized cases leads to SNR values around 5500 for integration times around 10–15 ms (SO) and 5–8 ms (LNO occultation), for one accumulation and for one pixel row of the detector. Considering that 160 ms corresponds to 7 accumulations, a further factor of about 2.6 is gained. Note that playing with the binning of rows, the SNR can still be improved (by a factor of $\sqrt{6} \sim 2.5$ at maximum). However we have considered a very conservative SNR value of 2000 for the determination of the detection limits. By choosing this low value, we expect to include the effect of the aerosols. For LNO in solar occultation, a similar reasoning led us to the value of 3000. As for LNO observations in nadir we considered a SNR value of 100. For the UVIS instrument, the value of 500 has been considered for both the solar occultation and the nadir observations. These noise values account for the instrument. From one simulated spectrum, 200 (for all UVIS geometries, and for SO and LNO solar occultation) or 100 (LNO nadir) noisy spectra were constructed by adding random noise corresponding to the selected SNR values. For example, in the case of UVIS nadir, a total of 3200 spectra ($=16$ different factors $\times$ 200 noisy spectra) were created for each target species.

The retrieval method was then applied to all these spectra and the retrieved quantities were compared to the initial abundances. The optical working principle of the SO and LNO channels is based on the combination of an echelle grating, used as a diffractive element, and an acousto-optical tunable filter, used as a diffraction order sorter. Therefore, the spectral range is measured using short spectral intervals corresponding to the diffraction orders. The width of the selected spectral windows varies from 20 to 35 cm^{-1} depending on the selected diffraction order. The correspondence between orders and spectral ranges covered has been described in Neefs et al. (2015). For each species, we have considered different orders to also have an indication on which would be the optimal setting for the detection of the target. For UVIS, the retrieval has been carried out considering the complete 200–650 nm spectral range since the instrument will always record the entire range.

For example, Fig. 2 shows the different diffraction orders that can be used to study the CH_4 band. The reference atmosphere described in the Table 2 is shown in grey while the ν_3 absorption band of methane is shown in red. This plot represents a spectrum

Table 3
Detection limits (ppb) for all the selected molecules using SO and LNO in solar occultation when individual orders are considered. The two lowest detection limits for methane are indicated in bold.

Species	Order	Wavenumber range cm^{-1}	Detection limits (ppb)	
			SO Channel SNR=2000	LNO Channel SNR=3000
CH_4	131	[2945 - 2968]	0.09	0.06
CH_4	132	[2967 - 2991]	0.045	0.045
CH_4	133	[2989 - 3013]	0.18	0.15
CH_4	134	[3012 - 3036]	**0.025**	**0.018**
CH_4	135	[3034 - 3059]	0.03	0.027
CH_4	136	[3057 - 3082]	**0.024**	**0.018**
CH_4	137	[3079 - 3104]	0.045	0.03
CH_4	138	[3102 - 3127]	0.09	0.1
C_2H_2	144	[3237 - 3263]	0.06	0.045
C_2H_2	145	[3259 - 3285]	0.03	0.027
C_2H_2	146	[3282 - 3308]	0.03	0.027
C_2H_2	147	[3304 - 3331]	0.03	0.03
C_2H_2	148	[3327 - 3353]	0.1	0.15
C_2H_4	131	[2945 - 2968]	0.3	0.30
C_2H_4	132	[2967 - 2991]	0.2	0.12
C_2H_4	133	[2989 - 3013]	0.2	0.20
C_2H_4	136	[3057 - 3081]	0.2	0.18
C_2H_4	137	[3079 - 3104]	0.2	0.15
C_2H_4	138	[3102 - 3127]	0.2	0.15
C_2H_4	139	[3124 - 3149]	0.15	0.15
C_2H_4	140	[3147 - 3172]	0.4	0.3
C_2H_4	141	[3169 - 3195]	0.75	0.6
C_2H_6	132	[2967 - 2991]	0.02	0.015
C_2H_6	133	[2989 - 3013]	0.03	0.018
CO	186	[4181 - 4214]	5.0	4.0
CO	187	[4203 - 4237]	2.0	2.0
CO	188	[4226 - 4260]	1.5	1.5
CO	189	[4248 - 4282]	1.5	1.5
CO	190	[4271 - 4305]	1.5	1.5
CO	191	[4294 - 4328]	2.5	2.5
HCl	125	[2810 - 2832]	0.05	0.06

Table 3 (*continued*)

HCl	126	[2832 - 2855]	0.06	0.04
HCl	129	[2899 - 2923]	0.07	0.05
HCl	130	[2922 - 2945]	0.03	0.025
HCl	131	[2944 - 2968]	0.03	0.03
HCN	145	[3259 - 3285]	0.06	0.05
HCN	146	[3282 - 3308]	0.03	0.03
HCN	147	[3304 - 3331]	0.05	0.03
HCN	148	[3327 - 3353]	0.04	0.025
H_2CO	122	[2742 - 2764]	0.05	0.04
H_2CO	123	[2765 - 2787]	0.045	0.04
H_2CO	124	[2787 - 2810]	0.04	0.03
H_2CO	125	[2810 - 2832]	0.045	0.04
H_2CO	126	[2832 - 2855]	0.075	0.045
H_2CO	127	[2855 - 2877]	0.045	0.04
H_2CO	128	[2877 - 2900]	0.06	0.045
H_2CO	129	[2899 - 2923]	0.1	0.075
HDO	118	[2652 - 2674]	1.8	1.6
HDO	119	[2675 - 2696]	1.5	1.2
HDO	120	[2697 - 2719]	4.5	3.5
HDO	121	[2720 - 2742]	1.4	1.1
HDO	122	[2742 - 2764]	1.8	1.6
HDO	123	[2765 - 2787]	1.4	1.4
H_2O	163	[3664 - 3693]	0.6	0.7
H_2O	166	[3731 - 3761]	0.3	0.25
H_2O	167	[3754 - 3784]	0.3	0.2
H_2O	168	[3776 - 3806]	0.25	0.25
H_2O	169	[3799 - 3829]	0.2	0.15
H_2O	170	[3821 - 3852]	0.2	0.15
H_2O	171	[3844 - 3874]	0.2	0.15
H_2O	172	[3866 - 3897]	0.5	0.4
H_2O	173	[3888 - 3920]	0.6	0.5
HO_2	151	[3394 - 3421]	1.5	1.0
HO_2	153	[3439 - 3467]	1	0.9
HO_2	156	[3506 - 3535]	4	2.5
H_2S	167	[3754 - 3784]	6.0	5.0
H_2S	168	[3776 - 3806]	4.0	4.0
H_2S	169	[3799 - 3829]	5.0	3.0
H_2S	170	[3821 - 3852]	3.0	3.0
N_2O	153	[3439 - 3467]	0.4	0.3
N_2O	154	[3461 - 3489]	0.2	0.2
N_2O	155	[3484 - 3512]	0.2	0.2

Table 3 (*continued*)

N_2O	195	[4383 - 4418]	1.0	4.0
N_2O	196	[4406 - 4441]	5.0	2.5
NO_2	128	[2877 - 2900]	0.20	0.14
NO_2	129	[2899 - 2923]	0.14	0.1
O_3	134	[3012 - 3036]	4.0	2.0
O_3	135	[3034 - 3059]	2.5	1.5
OCS	129	[2899 - 2923]	0.3	0.3
OCS	130	[2922 - 2945]	0.3	0.3

Table 4
Detection limits for solar occultation observations.

Species	SO	LNO	UVIS
CH_4	25 ppt	20 ppt	
C_2H_2	0.03 ppb	0.03 ppb	
C_2H_4	0.2 ppb	0.15 ppb	
C_2H_6	0.03 ppb	0.02 ppb	
CO	5 ppb	4 ppb	
HCl	0.03 ppb	0.025 ppb	
HCN	0.03 ppb	0.03 ppb	
H_2CO	0.04 ppb	0.03 ppb	7.5 ppb
HDO	0.7 ppb	0.7 ppb	
H_2O	0.2 ppb	0.15 ppb	
HO_2	1 ppb	1 ppb	
H_2S	4 ppb	3 ppb	
NH_3	–	–	1.0 ppb
N_2O	0.2 ppb	0.2 ppb	
NO_2	0.14 ppb	0.1 ppb	
O_3	2.5 ppb	1.5 ppb	50 ppt
OCS	0.3 ppb	0.3 ppb	
SO_2	–	–	0.5 ppb

obtained by the SO channel at 20 km altitude. For this molecule, we considered the orders 131 to 136 to estimate the detection limits, as it will be explained further.

3.1. Solar occultation geometry

After the addition of the noise, the retrieval was performed using the Levenberg–Marquardt inversion method, the starting point of which was randomly chosen within 30% around the reference concentration. This value was chosen in order to start from random values, but not too far away from the solution. Again the present study is focused on the determination of detection limits and not on the convergence characteristics of the retrieval code.

Typical results coming out of the procedure explained just above are shown in Fig. 3 for the methane detection for two different orders (131: 2944.5–2968.1 cm^{-1}; and 136: 3056.9–3081.4 cm^{-1}). In these plots, each dot represents a retrieved/initial abundance couple. One sees that when the abundance is high enough, i.e. well above the detection limit, there is no problem to retrieve the initial value. However when the initial abundance gets lower, the error increases as well as the spread of the results. The red dots are the average of the 200 values for each different factor. The average of the retrieved values, together with the associated error, are represented by the red curves. The blue lines represent the 1-sigma standard deviation of the 200 values. The detection limit is indicated by the arrow and is the lowest abundance for which the mean error is still lower than the standard deviation. Clearly, order 136 leads to a lower detection limit and would be a better choice to detect methane than order 131. Table 3 shows the detection limits of methane which have been inferred with this method for a series of orders and for SO and LNO operating in solar occultation. The best settings would be order 134 (which includes the Q branch and R(0) line of the ν_3 transition) and 136 (which includes the intense R(3) to R(5) lines of the same band).

The same procedure has been applied for all the species mentioned in Table 2. The different spectral intervals and detection limits are reported in Table 3. HDO detection limits values have been obtained from the retrieved H_2O density considering the isotopic ratio of 5.6 VSMOW at Mars (Krasnopolsky, 1997; Lodders and Fegley, 1997; Owen et al., 1977). A similar analysis has been performed for the species absorbing in the UVIS spectral range, i.e. O_3, SO_2, H_2CO and NH_3. The detection limits are reported in Table 4.

The values reported in Table 3 are essentially modulated by the line intensity in each of the spectral interval, and indicate which order to select for the optimum detection of each species. Moreover, they can be used to choose specific orders containing sufficient information on several species and that can then be observed simultaneously. For example, selecting order 129 for HCl, whilst not the optimal one for that species, would also allow the possible detection of H_2CO, OCS and NO_2, or at least the determination of upper limits. The detection limits for the three channels in the solar occultation mode are summarized in Table 4 for the different species targeted in this study.

3.2. Nadir observation geometry

A similar analysis has been performed for nadir observation, with LNO and UVIS. The retrieval of nadir spectra is not as straightforward as for the solar occultation cases. Here we used the Optimal Estimation method (OEM) developed by Rodgers (2000) to derive the column density of the target species. In this method, an a priori abundance and variability have to be provided. One of the parameters generated by the OEM is the degree of freedom for signal, or DOFS, which indicates how many pieces of information can be extracted independently from the retrieval. If the DOFS is zero, no information was found in the spectrum (it was too noisy and/or the abundance too small), the answer will be the a priori value ingested in the OEM, whereas a DOFS of 1 indicates a retrieval where information could be found in the spectrum (the absorption signature is well above the noise level). In nadir retrievals, the DOFS seems to be the most interesting parameter to look at to determine the detection limit. Considering the following criterion: “the detection limit corresponds to the abundance for which DOFS is equal to 0.5”, we produced detection limit values for the different species considered in this study. The value of 0.5 has been chosen as it resulted in an error on the retrieved values lower than 20%. This threshold was chosen empirically. An example is given in Fig. 4.

If we apply this criterion on the O_3 detection with UVIS, we see that the abundance corresponding to a DOFS of 0.5 is 4.5 ppb (see Fig. 5). In this figure, the different individuals DOFS values are plotted as a

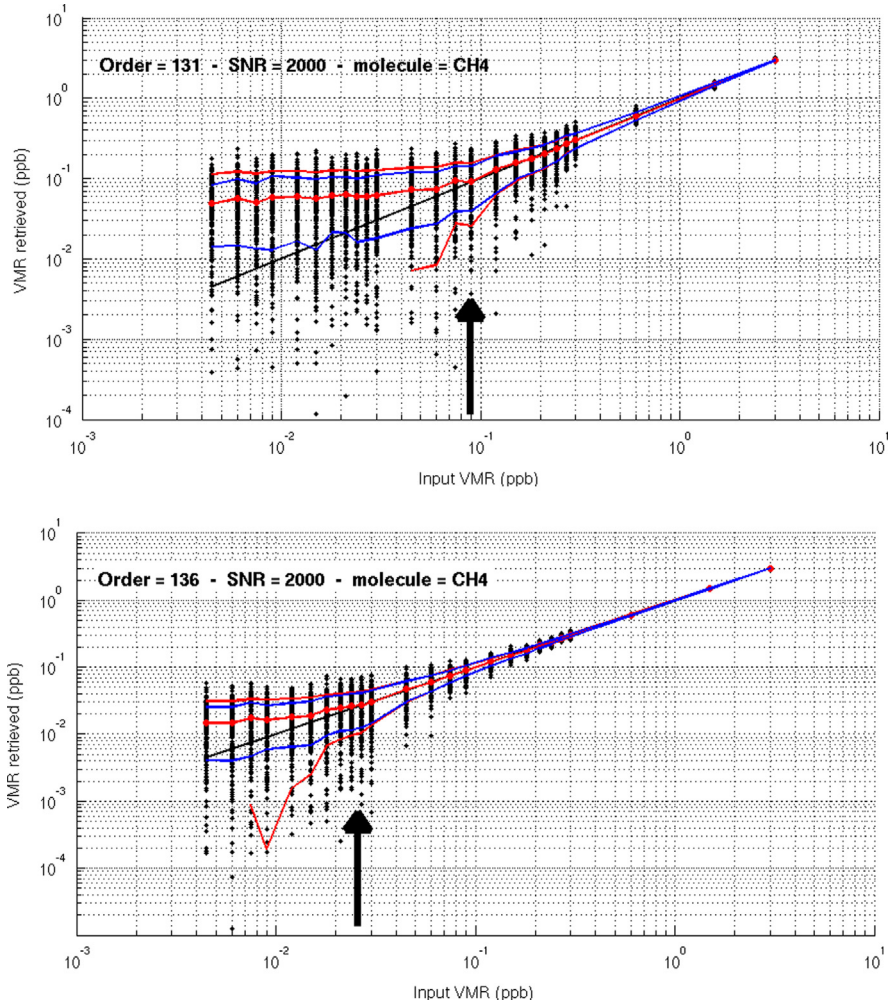

Fig. 3. Example of results in the case of methane: (top) for the order 131 (2944.5–2968.1 cm−1) and (bottom) for the order 136 (3056.9–3081.4 cm−1). The black dots are the individual (initial-retrieved) abundances of CH4; the red circles are the average retrieved value for each injected abundance; the red curves are the retrieved average +/− the average error on the retrievals; the blue curves are the retrieved averages +/− the standard deviation of the retrieved values and the black line represent the ideal retrieval (=injected value). The arrows indicate the detection limit values when the average error starts to be larger than the standard deviation. (For interpretation of the references to color in this figure legend, the reader is referred to the web version of this article.)

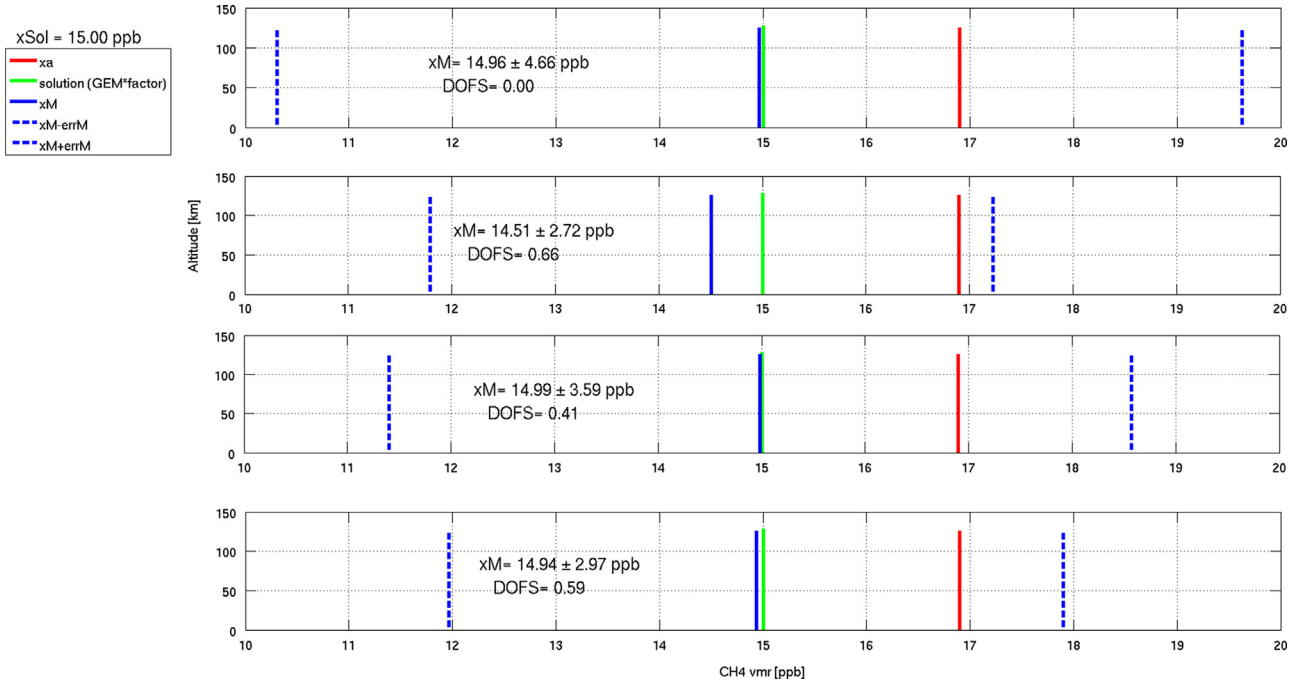

Fig. 4. Results of the retrievals of CH_4 with LNO NADIR. The seven plots represent the seven spectral windows tested (orders 133–136, from top to bottom). For each plot, the red line represents the a priori volume mixing ratio used for the retrievals. In blue are represented the retrieved value (p plain) and its error (dotted). The green line is the expected value if the retrieval was successful (xSol = 15 ppb here). The retrieved value (xM) with its error and the DOFS of the retrieval are also indicated. As can be seen on the first panel, even with a DOFS of 0.0, ASIMUT-ALVL reaches the solution. As this is not reliable, a more selective criterion has been applied: the DOFS must be > 0.5, this implies an error of less than 20%, as can be calculated from all panels given here. (For interpretation of the references to color in this figure legend, the reader is referred to the web version of this article.)

function of the initial abundance (dots). The red curve represents the average DOFS value obtained for a given initial abundance. At high abundances, DOFS values are equal to 1, meaning that the retrieval was successful and could derive information out of the noisy spectra. On the contrary, at lower abundances, the noise overwhelms the target signature and no information could be driven out of the spectra.

A similar procedure was applied for the other species absorbing in the UV (Table 4) and the ones absorbing in the IR using the LNO channel. In the UV region, it was however impossible to derive detection limit for NH_3. This is not unexpected since the absorption of this species occurs near the 200 nm extremity of the UVIS spectrum where the signal and SNR are low.

Table 5
Best detection limits for the LNO channel per molecule for some of the tested orders.

Species	Diffraction order	Detection limit	Species	Diffraction order	Detection limit
CH_4	134	11 ppb	H_2O	168	51 ppb
	135	19 ppb		169	31 ppb
	136	13 ppb		170; 171	47 ppb
CO	188	2.2 ppm	HDO	119	1.3 ppm
	189	2.1 ppm		121	0.8 ppm
	190	1.5 ppm		123	1.0 ppm
HCl	129	312 ppb	HCN	146	19 ppb
	130	31 ppb		147	21 ppb
	131	73 ppb		148	15 ppb
C_2H_2	145; 146	20 ppb	C_2H_6	132	11 ppb
	147	21 ppb		133	14 ppb
C_2H_4	132	70 ppb	H_2CO	123	21 ppb
	137	90 ppb		124	16 ppb
	139	80 ppb		125	20 ppb
HO_2	151; 153	0.5 ppm	H_2S	168 ; 169	2.1 ppm
	156	1 ppm		170	1.6 ppm
NO_2	128	75 ppb	OCS	129	122 ppb
	129	50 ppb		130	131 ppb
N_2O	153	159 ppb	O_3	135	0.8 ppm
	154	83 ppb			
	155	88 ppb			

As for the SO and LNO solar occultation results, detection limit values are specified for different orders (spectral intervals) for the LNO nadir simulations (Table 5). The OEM was used to characterize the detection limits achievable with the LNO channel in nadir observation mode for 17 molecules. 50 factors, from 0.001 to 100 were applied to the initial values presented in Table 2. Random noise was added to the simulated spectra in order to create a batch of 100 spectra per factor per molecule. Using that methodology, we know what to expect from the retrieval, i.e. the retrieved density should equal the initial density value times the factor considered in that particular case. The retrievals were run with ASIMUT-ALVL using a random a priori value of 30% around the solution and a variability of 10%. Several orders of diffraction were considered in order to find out the best spectral ranges to study. For each molecule and each order, the values of the DOFS for the 5000 retrievals, i.e. 50 factors times 100 spectra, were plotted (red dots in Fig. 6). According to the criterion stated earlier in this section, the detection limits were determined using the DOFS values. Two examples are given in the Fig. 6 for CH_4.

One order of magnitude difference is obtained for the detection limit of the two orders presented in Fig. 6. DOFS = 0.5 for a density of 110 ppb in the order 133 (on the left of Fig. 6) while 11 ppb is detectable in the order 134 (on the right of Fig. 6). The detection limits for some of the orders are given in the Table 5 while Table 6 only indicates the lowest detection limit. As for solar occultation, HDO detection limits values have been obtained from the retrieved H_2O density using the Martian isotopic ratio of 5.6 VSMOW (Krasnopolsky, 1997; Lodders and Fegley, 1997; Owen et al., 1977).

These detection limits are within the expected range considering the SNR value (100) of the LNO channel. Our current knowledge of some of the species will be improved, especially for H_2O, CO, C_2H_4, C_2H_6. For CH_4, we do not reach the 7 ppb limit established by Curiosity (Webster et al., 2015) but the value of 11 ppb is still valuable considering the other detections that were published earlier. One way to improve this detection limit will be of course, to average several observations, although the spatial resolution will then be impacted.

4. Conclusions

NOMAD is a spectrometer suite that is part of the ExoMars mission towards Mars. It is composed of three channels, operating in the UV and IR spectral ranges and performing solar occultation and nadir observations. Although other pointing capabilities, e.g. limb, are possible with the instrument, they are not part of the current baseline activities of the spacecraft.

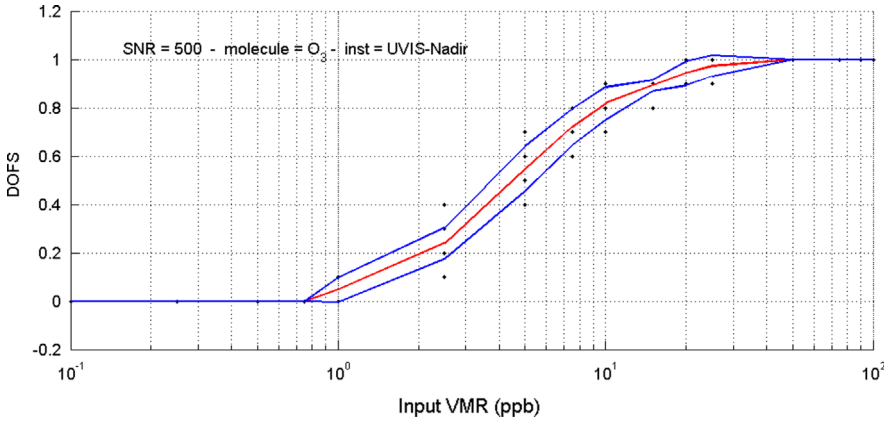

Fig. 5. DOFS criterion applied to the O_3 detection. The red curve represents the average DOFS value obtained for a given initial abundance and the blue curves the 2-sigma standard deviation. (For interpretation of the references to color in this figure legend, the reader is referred to the web version of this article.)

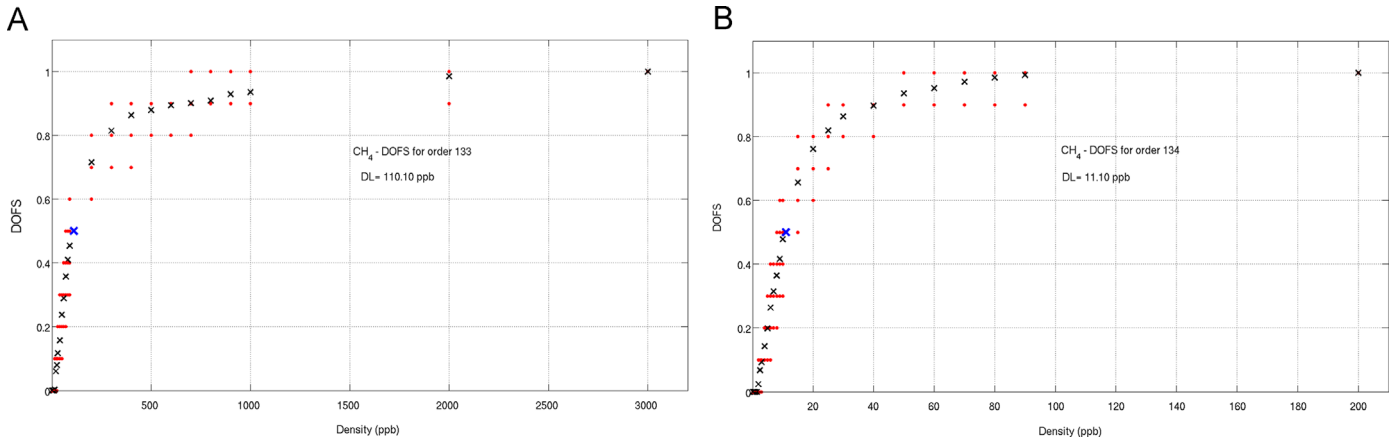

Fig. 6. Degree of freedom for Signal of the retrievals in the LNO diffraction order 133 (2989.416–3013.415 cm−1) and order 134 (3011.893–3036.072 cm−1) for CH4. The red dots correspond to each individual retrieval. The black crosses represent the averages of the DOFS for each considered factor. The blue cross indicates the value of DOFS=0.5 hence the value of the detection limit in abscissa, in ppb. (For interpretation of the references to color in this figure legend, the reader is referred to the web version of this article.)

Table 6
Detection limits for LNO and UVIS nadir observations.

Species	LNO	UVIS
CH_4	11 ppb	
C_2H_2	20 ppb	
C_2H_4	70 ppb	
C_2H_6	11 ppb	
CO	1.5 ppm	
HCl	31 ppb	
HCN	15 ppb	
H_2CO	16 ppb	150 ppb
HDO	0.7 ppm	
H_2O	31 ppb	
HO_2	0.5 ppm	
H_2S	1.6 ppm	
NH_3	–	–
N_2O	83 ppb	
NO_2	50 ppb	
O_3	0.8 ppm	4.5 ppb
OCS	122 ppb	
SO_2	–	18 ppb

We have shown that the instrument will be capable of measuring a large suite of species that are/or could be present in the atmosphere of Mars. The solar occultation technique is a very powerful observational method: it is a self-calibrated method (the full Sun reference spectrum is measured outside of the atmosphere during each occultation and transmittances that are free of solar lines are analyzed) allowing for the retrieval of high spatial vertical profiles of the target molecules from the upper layers of the atmosphere down to the surface or near-surface depending on the loading in dust and particles. The nadir observations will provide maps of a series of constituents leading to the determination of sources and sinks, as well as put constraints on some surface processes. Sub-ppb level of methane, <25 parts per trillion (ppt), are detectable by the instrument in solar occultation mode and 11 parts per billion in nadir mode.

Although the analysis has been carried out on the latest version of the channels' SNR models containing the updated characteristics of the optical elements, this remains a theoretical exercise that will be re-evaluated when calibration data will be available. This may take place either after the analysis and interpretation of the measurement made in the laboratory just before delivery of the instrument to ESA, or in-flight. The impacts of dust loading on the detection limits of the channels will be investigated in a follow-up study. The true performances however, will be known only be revealed when the first Martian measurements are performed.

Acknowledgments

The NOMAD instrument has been developed under the responsibility of a Belgian principal investigator team (IASB-BIRA, Brussels), assisted by Co-PI teams from Spain (IAA-CSIC, Granada) and the United Kingdom (OU, Milton-Keynes). Associated teams contributing to the design and development of NOMAD were CSL (Liège, Belgium), IAPS (Rome, Italy) and IDR-UPM (Madrid, Spain). We thank all engineering and supporting personnel in these teams. Several industrial partners were associated to the abovementioned teams. The industrial efforts were coordinated by a Belgian prime contractor (OIP, Oudenaarde). The UVIS channel was developed by Lambda-X (Nivelles, Belgium).

NOMAD has been made possible thanks to funding by the Belgian Science Policy Office (BELSPO) and financial and contractual coordination by the ESA Prodex Office (PlanetADAM no 4000107727). The research was performed as part of the "Inter-university Attraction Poles" programme financed by the Belgian Government (Planet TOPERS no P7-15) and a BRAIN Research Grant BR/143/A2/SCOOP. The research leading to these results has received funding from the European Community's Seventh Framework Programme (FP7/2007-2013) under Grant Agreement no. 607177 CrossDrive. UK funding is acknowledged under the UK Space Agency Grant ST/I003061/1.

The NOMAD Team – Science Team: Vandaele A.C.; Lopez Moreno J.J.; Bellucci G.; Patel M.; Allen M.; Altieri F.; Aoki S.; Bolsée D.; Clancy T.; Cloutis E.; Daerden, F.; Depiesse C.; Fedorova A.; Formisano V.; Funke B.; Fussen D.; Garcia-Comas M.; Geminale A.; Gérard J.-C.; Gillotay D.; Giuranna M.; Gonzalez-Galindo F.; Ignatiev N.; Kaminski J.; Karatekin O.; Kasaba, Y.; Lefèvre F.; Lewis, S.; López-Puertas M.; López-Valverde M.; Mahieux A.; Mason J.; McConnell, J.(†); Mumma M.; Neary L.; Neefs E.; Novak, R.; Renotte E.; Robert S.; Sindoni G.; Smith M.; Thomas I.R.; Trokhimovskiy A.; Vander Auwera J.; Villanueva G.; Viscardy, S.; Whiteway J.; Willame Y.; Wilquet V.; Wolff M. **- Tech Team:** Alonso-Rodrigo G.; Aparicio del Moral B.; Barzin P.; BenMoussa A.; Berkenbosch S.; Biondi D.; Bonnewijn S.; Candini G.; Clairquin R.; Cubas J.; Delanoye S.; Giordanengo B.; Gissot S.; Gomez A.; Zafra J.-J.; Leese M.; Maes J.; Mazy E.; Mazzoli A.; Meseguer J.; Morales R.; Orban A.; Pastor-Morales M.; Perez-Grande I.; Ristic B.; Rodriguez-Gomez J.; Saggin B.; Samain V.; Sanz Andres A.; Sanz R.; Simar J.-F.; Thibert T.

References

Brion, J., et al., 1993. High-resolution laboratory absorption cross section of O_3. Temperature effect. Chem. Phys. Lett. 213 (5/6), 610–612.

Bolsée, D., 2012. Métrologie de la Spectrophotométrie Solaire Absolue : Principes, Mise en œuvre et Résultats. Instrument SOLSPEC à bord de la Station Spatiale Internationale. Univ. Brussels.

Bolsée, D., et al., 2016. SOLAR/SOLSPEC mission on ISS: in-flight performances for SSI measurements in the UV. Astron. Astrophys. (in preparation)

Chance, K., Orphal, J., 2011. Revised ultraviolet absorption cross sections of H_2CO for the HITRAN database. J. Quant. Spectrosc. Radiat. Transf. 112, 1509–1510.

Cheng, B.-M., et al., 2006. Absorption cross sections of NH_3, NH_2D, NHD_2, and ND_3 in the spectral range 140–220 nm and implications for planetary isotopic fractionation. Astrophys. J. 647, 1535–1542.

Drummond, R., et al., 2011. Studying methane and other trace species in the Mars atmosphere using a SOIR instrument. Planet. Space Sci. 59, 292–298.

Daerden, F., et al., 2015. A solar escalator on Mars: self-lifting of dust layers by radiative heating. Geophys. Res. Lett. 42 (18), 7319–7326.

Danielache, S.O., et al., 2008. High-precision spectroscopy of ^{32}S, ^{33}S, and ^{34}S sulfur dioxide: ultraviolet absorption cross sections and isotope effects. J. Geophys. Res. 113 (D17314), 1–14. http://dx.doi.org/10.1029/2007JD009695.

Daumont, D., et al., 1992. Ozone UV spectroscopy I: absorption cross-sections at room temperature. J. Atmos. Chem. 15 (2), 145–155.

Encrenaz, T., et al., 2011. A stringent upper limit to SO_2 in the Martian atmosphere. Astron. Astrophys. 530, A37.

Fedorova, A., et al., 2009. Solar infrared occultation observations by SPICAM experiment on Mars-Express: simultaneous measurements of the vertical distributions of H_2O, CO_2 and aerosol. Icarus 200 (1), 96–117.

Formisano, V., et al., 2004. Detection of methane in the atmosphere of Mars. Science 306, 1758–1761.

Gallery, W.O., Kneizys, F.X., Clough, S.A., 1983. Air Mass Computer Program for Atmospheric Transmittance/Radiance Calculation: FSCATM. H.A. Air Force Geophysical Laboratory, MA, Air Force.

Huestis, D.L., Berkowitz, J., 2011. Critical evaluation of the photoabsorption cross section of CO2 from 0.125 to 201.6 nm at room temperature. Adv. Geosci.: Planet. Sci. 25, 229–242. http://dx.doi.org/10.1142/9789814355377_0018.

Hartogh, P., et al., 2010. Herschel/HIFI observations of Mars: first detection of O_2 at submillimetre wavelengths and upper limits on HCl and H_2O_2. Astron. Astrophys. 521 (L49). http://dx.doi.org/10.1051/0004-6361/201015160.

Hermans, C., Vandaele, A.C., Fally, S., 2009. Fourier Transform measurements of SO_2 absorption cross sections: I. Temperature dependence in the 24,000–29,000 cm^{-1} (345–420 nm) region. J. Quant. Spectrosc. Radiat. Transf. 110, 756–765.

Hase, F., et al., 2010. The ACE-FTS atlas of the infrared solar spectrum. J. Quant. Spectrosc. Radiat. Transf. 111 (4), 521–528.

Kochenova, S., et al., 2011. ALVL 1.0: an advanced line-by-line radiative transfer model for the retrieval of atmospheric constituents from satellite and ground-based measurements. In: Proceedings of International Symposium "Atmospheric Radiation and Dynamics". St. Petersbourg, Russia.

Krasnopolsky, V.A., Maillard, J.P., Owen, T.C., 2004. Detection of methane in the Martian atmosphere: evidence for life? Icarus 172 (2), 537–547.

Krasnopolsky, V.A., 2005. A sensitive search for SO_2 in the martian atmosphere: implications for seepage and origin of methane. Icarus 178 (2), 487–492.

Krasnopolsky, V.A., 1997. High-resolution spectroscopy of Mars at 3.7 and 8 microm: a sensitive search for H_2O_2, H_2CO, HCl, and CH_4, and detection of HDO. J. Geophys. Res. 102 (E3), 6525–6534.

Lefevre, F., et al., 2004. Three-dimensional modeling of ozone on Mars. J. Geophys. Res. 109. http://dx.doi.org/10.1029/2004JE002268.

Lodders, K., Fegley, B., 1997. An oxygen isotope model for the composition of mars. Icarus 126 (2), 373–394.

Maguire, W.C., 1977. Martian isotopic ratios and upper limits for possible minor constituents as derived from Mariner 9 infrared spectrometer data. Icarus 32 (1), 85–97.

Mahieux, A., et al., 2009. A new method for determining the transfer function of an acousto optical tunable filter. Opt. Express 17, 2005–2014.

Mishchenko, M.I., Travis, L.D., 1998. Capabilities and limitations of a current Fortran implementation of the T-matrix method for randomly oriented, rotationally symmetric scatterers. J. Quant. Spectrosc. Radiat. Transf. 60 (3), 309–324.

Meller, R., Moortgat, G.K., 2000. Temperature dependence of the absorption cross sections of formaldehyde between 223 and 323 K in the wavelength range 225–375 nm. J. Geophys. Res. 105 (D6), 7089–7101.

Mahaffy, P.R., et al., 2013. Abundance and isotopic composition of gases in the Martian atmosphere from the Curiosity Rover. Science 341, 263–266.

Malicet, J., et al., 1995. Ozone UV spectroscopy. II. Absorption cross-sections and temperature dependence. J. Atmos. Chem. 21 (3), 263–273.

Mumma, M.J., et al., 2009. Strong release of methane on Mars in Northern Summer 2003. Science 323 (5917), 1041–1045.

Nakagawa, H., et al., 2009. Search of SO_2 in the Martian atmosphere by ground-based submillimeter observation. Planet. Space Sci. 57 (14-15), 2123–2127.

Neefs, E., et al., 2015. NOMAD spectrometer on the ExoMars trace gas orbiter mission: part 1—design, manufacturing and testing of the infrared channels. Appl. Opt. 54 (28), 8494–8520.

Owen, T., et al., 1977. The composition of the atmosphere at the surface of Mars. J. Geophys. Res. 82, 4635–4639.

Patel, M.R., et al., 2007. UVIS: the UV–vis spectrometer for the ExoMars mission. In: Proceedings of European Mars Science and Exploration Conference: Mars Express & ExoMars. ESTEC, Noordwijk, The Netherlands.

Parkinson, W.H., Rufus, J., Yoshino, K., 2003. Absolute absorption cross section measurements of CO_2 in the wavelength region 163–200 nm and the temperature dependence. Chem. Phys. 290 (2–3), 251–256.

Perrier, S., et al., 2006. Global distribution of total ozone on Mars from SPICAM/MEX UV measurements. J. Geophys. Res. 11. http://dx.doi.org/10.1029/2006JE002681.

Rodgers, C.D., 2000. Inverse methods for atmospheric sounding: theory and practice. In: Hackensack, N.J. (Ed.), World Scientific. University of Oxford, Oxford.

Rothman, L.S., et al., 2013. The HITRAN2012 molecular spectroscopic database. J. Quant. Spectrosc. Radiat. Transf. 130, 4.

Spurr, R.J.D., 2006. VLIDORT: a linearized pseudo-spherical vector discrete ordinate radiative transfer code for forward model and retrieval studies in multilayer multiple scattering media. J. Quant. Spectrosc. Radiat. Transf. 102, 316–342.

Serdyuchenko, A., et al., 2014. High spectral resolution ozone absorption cross-sections – Part 2: temperature dependence. Atmos. Meas. Tech. 7, 625–636.

Sander, S.P., et al., 2011. Chemical Kinetics and Photochemical Data for Use in Atmospheric Studies, Evaluation no. 17, J.P.L. JPL Publication 10–6, Pasadena, USA. ⟨http://jpldataeval.jpl.nasa.gov⟩.

Smith, M.D., 2004. Interannual variability in TES atmospheric observations of Mars during 1999–2003. Icarus 167 (1), 148–165.

Smith, M., et al., 2009. Compact Reconnaissance Imaging Spectrometer observations of water vapor and carbon monoxide. J. Geophys. Res. 114. http://dx.doi.org/10.1029/2008JE003288.

Sneep, M., Ubachs, W., 2005. Direct measurement of the Rayleigh scattering cross section in various gases. J. Quant. Spectrosc. Radiat. Transf. 92 (3), 293–310.

Thomas, I.R., Vandaele, A.C., Robert, S., Neefs, E., Drummond, R., Daerden, F., Delanoye, S., Ristic, B., Berkenbosch, S., Clairquin, R., Maes, J., Bonnewijn, S., Depiesse, C., Mahieux, A., Trompet, L., Neary, L., Willame, Y., Wilquet, V., Nevejans, D., Aballea, L., Moelans, W., De Vos, L., Lesschaeve, S., Van Vooren, N., Lopez-Moreno, J.-J., Patel, M.R., Bellucci, G., 2016. the NOMAD Team, Optical and radiometric models of the NOMAD instrument part II: the infrared channels–SO and LNO. Opt. Express 24 (4), 3790–3805.

Vandaele, A.C., Neefs, E., Drummond, R., Thomas, I.R., Daerden, F., Lopez-Moreno, J.-J., Rodriguez, J., Patel, M.R., Bellucci, G., Allen, M., Altieri, F., Bolsée, D., Clancy, T., Delanoye, S., Depiesse, C., Cloutis, E., Fedorova, A., Formisano, V., Funke, B., Fussen, D., Geminale, A., Gérard, J.-C., Giuranna, M., Ignatiev, N., Kaminski, J., Karatekin, O., Lefèvre, F., López-Puertas, M., López-Valverde, M., Mahieux, A., McConnell, J., Mumma, M., Neary, L., Renotte, E., Ristic, B., Robert, S., Smith, M., Trokhimovsky, S., Vander Auwera, J., Villanueva, G., Whiteway, J., Wilquet, V., Wolff, M., 2015a. and The NOMAD Team, Science objectives and performances of NOMAD, a spectrometer suite for the ExoMars TGO mission. Planet. Space Sci. 119, 233–249.

Vandaele, A.C., et al., 2015b. Optical and radiometric models of the NOMAD instrument part I: the UVIS channel. Opt. Express 23 (23), 30028–30042.

Vandaele, A.C., et al., 2008. Composition of the Venus mesosphere measured by SOIR on board Venus Express. J. Geophys. Res. 113. http://dx.doi.org/10.1029/2008JE003140.

Vandaele, A.C., Kruglanski, M., De Mazière, M., 2006. Modeling and retrieval of atmospheric spectra using ASIMUT. In: Proceedings of the First Atmospheric Science Conference. ESRIN, Frascati, Italy.

Vandaele, A.C., Hermans, C., Fally, S., 2009. Fourier Transform measurements of SO_2 absorption cross sections: II. temperature dependence in the 29,000–44,000 cm^{-1} (227–345 nm) region. J. Quant. Spectrosc. Radiat. Transf. 110, 2115–2126.

Villanueva, G.L., et al., 2013. A sensitive search for organics (CH_4, CH_3OH, H_2CO, C_2H_6, C_2H_2, C_2H_4), hydroperoxyl (HO_2), nitrogen compounds (N_2O, NH_3, HCN) and chlorine species (HCl, CH_3Cl) on Mars using ground-based high-resolution infrared spectroscopy. Icarus 223 (1), 11–27.

Wilquet, V., et al., 2009. Preliminary characterization of the upper haze by SPICAV/SOIR solar occultation in UV to mid-IR onboard Venus Express. J. Geophys. Res. 114, E00B42.

Wilquet, V., et al., 2012. Optical extinction due to aerosols in the upper haze of Venus: Four years of SOIR/VEX observations from 2006 to 2010. Icarus 217 (2), 875–881.

Webster, C., et al., 2015. Mars methane detection and variability at Gale crater. Science 347 (6220), 415–417.